The outskirt of the Virgo cD galaxy M87 as revealed by Planetary Nebulae

A.Longobardi
O.Gerhard
M.Arnaboldi

Max-Planck-Institut für extraterrestrische Physik

EWASS 2015, Sp16

Outer regions of galaxies and structure formation

- Formation of ICL and extended halos around BCGs closely related to the morphological transformation of galaxies in clusters
  - dynamical friction
  - tidal forces
- Simulations show that mergers and accretion are driving mechanisms for galaxy characteristics at the current epoch
- Outer regions of galaxies preserve fossil records of the accretion events that characterise the hierarchical assembly of galaxies
- From the study of the luminosity, distribution and kinematics of galaxy halos and ICL we get information on the evolution of galaxies and hosting clusters

BCG and ICL single entity or discrete components?

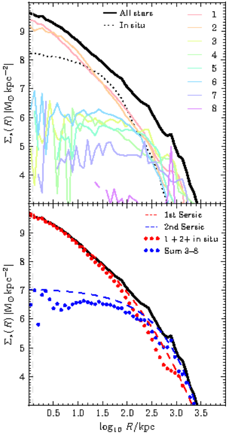

Single entity consisting of all stars not bound to any subhalos (Zibetti+05,D'Souza+14,Cooper+14)

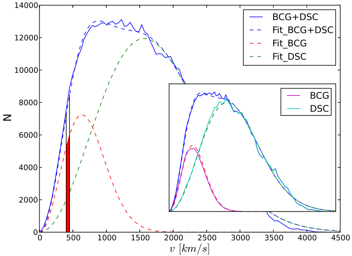

Two **distinct dynamical components** with different parent stellar systems in terms of spatial distribution, age and metallicity (Cui+14, Dolag+2010)

M87 and the Virgo Cluster

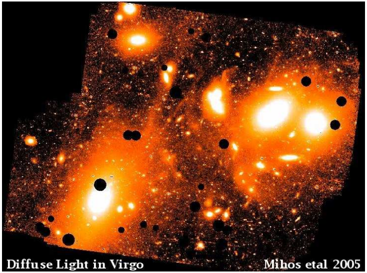

Ultra-deep wide field ($1.5^\circ \times 1.5^\circ$) image of the Virgo cluster core (Mihos et al. 2005)

- At the centre of the subcluster A in the Virgo cluster (Binggelli et al. 1987)
- Old stellar population (Liu et al 2005), not recent merger
- Extended stellar halo down to $\mu_V \sim 27.0$ mag arcsec^{-2} (Kormendy at al. 2009)
- Complex network of extended tidal features in the outer regions (Mihos et al. 2005)

Planetary Nebulae (PNe) as tracers

- Final stage of 1-8 $M_\odot$ at the end of the AGB phase
- Lifetime $\sim$ 10,000 yr
- Pulsation and radiation pressure cause mass loss via winds
- Strong UV flux
- Up to 15% of the UV emitted energy by the central star re-radiated in the [OIII] λ5007 emission line (Dopita et al. 1992)
- PNe as extragalactic distance indicators, due to the particular shape of their [OIII] λ5007 Planetary Nebulae Luminosity Function (PNLF)
- PNe powerful kinematic tools
- PNe tracers of light and stellar populations through the luminosity specific PN number, α parameter

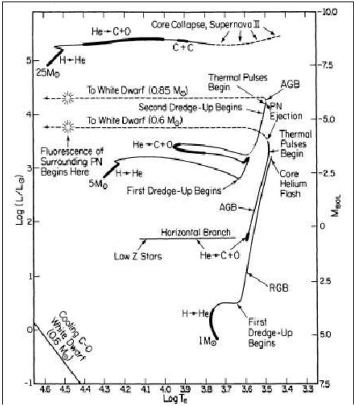

Suprime-Cam and FLAMES Surveys

Surveyed Area $\sim 0.5 \mathrm{deg}^2$

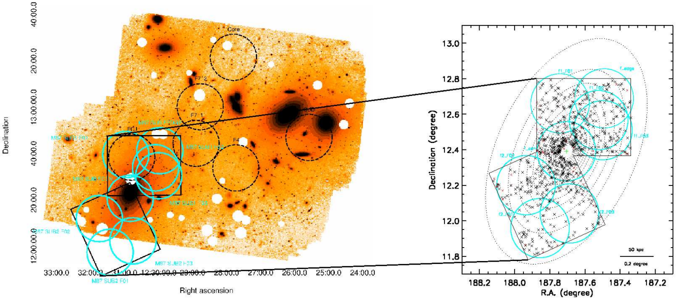

Suprime-Cam@Subaru Two fields covering the halo of M87 out to 150 kpc (FOV 34'×27') Fields observed through the NB503 narrow-band ([OIII] 5029 Å 74 Å) and broad-band V filter (Longobardi+13)

FLAMES@VLT
high-resolution grism HR08
$\lambda_c = 5048$Å
spectral resolution of 22 500
FWHM=0.29 Å (17 km/s)
λ_{err}= 0.0025 Å (150 m/s)
(Longobardi+15a)

Halo and ICL: Kinematical separation

The outskirt of the Virgo cD galaxy M87 as revealed by Planetary Nebulae

A.Longobardi O.Gerhard M.Arnaboldi

Introduction

Photometric and Spectroscopic surveys

PNe as tracers of light and stellar population

Summary

Sample of ~ 300 spectroscopically confirmed PNe out to 200 kpc

Red: halo PNe (bound)

Blue: intracluster PNe (unbound) Black squares: PN data from Doherty+09

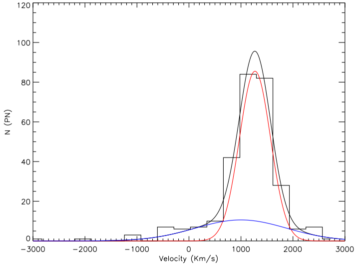

PN LOSVD for halo (red) and IC (blue) components (Longobardi+15a)

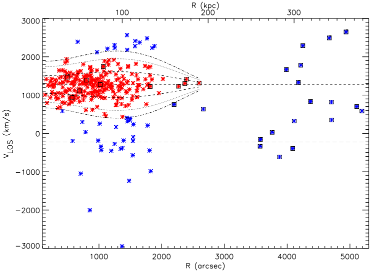

V_{LOS} vs major axis distance (Longobardi+15a)

- M87 halo and Virgo ICL are dynamically distinct components with different density profiles

PN Surface Density profile

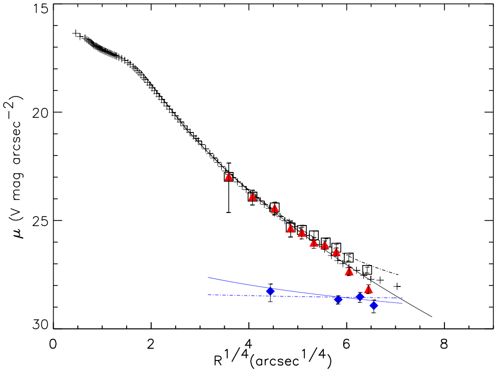

$$\mu_{\mathrm{PNe}}(R) = -2.5\log_{10}\left(\Sigma_{\mathrm{PNe}}(R)\right) + \mu_0$$

The halo component is more centrally concentrated and less extended than the ICL

Two component photometric model

$$\tilde{\Sigma}(R) = \alpha_{2,5,\mathrm{halo}} \left[I(R)_{K09} + \left(\frac{\alpha_{2,5,\mathrm{ICL}}}{\alpha_{2,5,\mathrm{halo}}} - 1 \right) I_{\mathrm{ICL}} \right]$$

$$\alpha_{\mathbf{2.5},\mathrm{halo}} = (\mathbf{1.07} \pm \mathbf{0.12}) \times \mathbf{10^{-8}} \mathrm{PNL}_{\odot}^{\mathbf{-1}}$$

$$\alpha_{\mathbf{2.5},\mathrm{ICL}} / \alpha_{\mathbf{2.5},\mathrm{halo}} \sim \mathbf{2.5}$$

$$\alpha_{\mathbf{2.5},\mathrm{ICL}} = (\mathbf{2.72} \pm \mathbf{0.63}) \times \mathbf{10^{-8}} \mathrm{PNL}_{\odot}^{\mathbf{-1}}$$

$$\mathbf{I}_{\mathrm{ICL}} \propto \mathbf{R}^{\gamma}$$

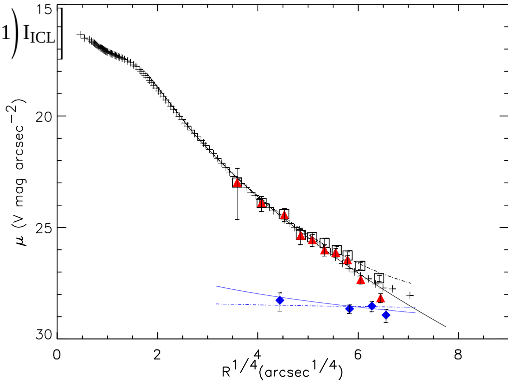

M87 azimuthally averaged colour profile becomes bluer at larger radii (Rudick+10) in the same regions where we observe the α parameter increment

If the stars in the M87 halo have a higher metallicity than the ICL, we might expect a variation of the luminosity specific PN number in the region of radii where the M87 stellar halo and the ICL are superposed along the LOS

M87 Planetary Nebula Luminosity Function

PNLF Analytical Formula

$$N(M) \propto e^{c_2 M}\left\{1 - e^{3(M^* - M)}\right\}$$

$c_2 = 0.307$

M^*(5007)=-4.5 mag

Ciardullo et al. 1989

- Reproduces the high mass cut-off
- Models the expansion of the envelope and the slow PN fading rate

M87 Planetary Nebula Luminosity Function

Red: halo PNLF
Blue : ICL PNLF
cyan triangles : M33 PNLF

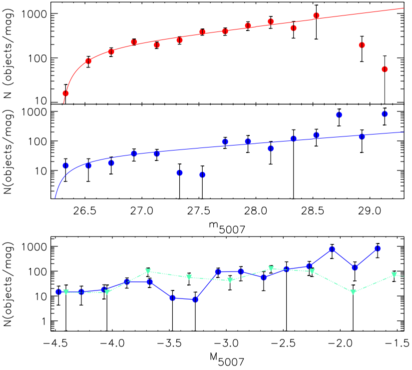

- Halo PNLF has steeper slope at fainter magnitude than ICPNLF
- Dip in the ICPNLF as observed for PN populations in star forming galaxies

M87 Halo Phase-space

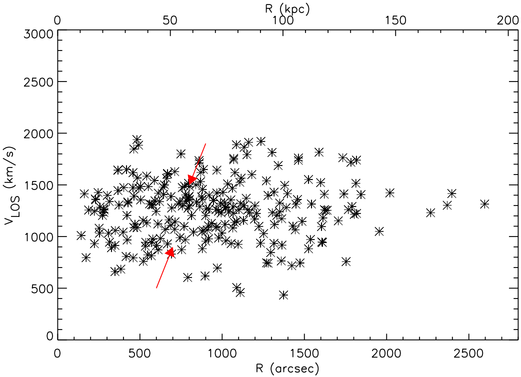

- The Halo phase-space shows a non uniform distribution of points
- Chevron-like substructure

PN tagging: Gaussian Mixture Models

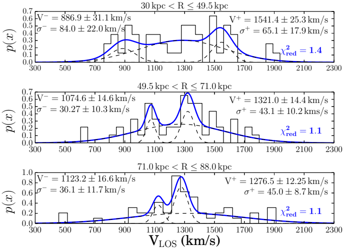

GMM assigns the contribution of each particle to the total (mixture) probability distribution

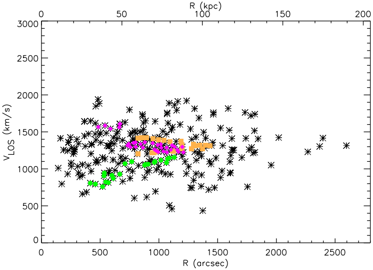

Chevron PNe (magenta, and green points; Longobardi+15c). Orange sqaures: GC substructure (Romanowsky+12)

- Chevron substructure extends over 700” along the major axis
- Asymmetry in number of PNe in the substructure

Chevron Spatial distribution and M87 surface brightness: The Crown of M87

PN overdensity associated to a substructure in Surface brightness

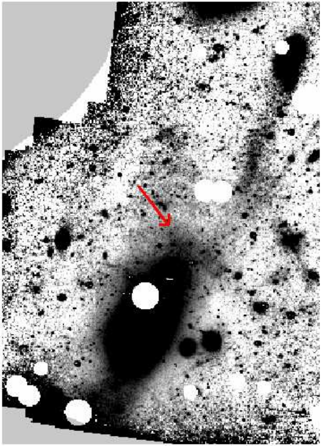

Masked Image that amplifies the high-frequency components.

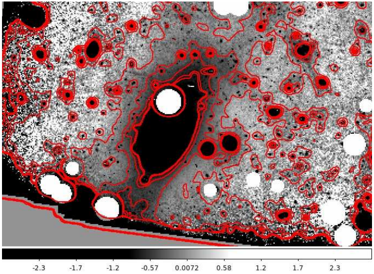

Contours map on the unsharped masked image.
Contours go from -0.1 to -0.8 in steps of 0.2

Longobardi+15c

Chevron Spatial distribution and M87 colour

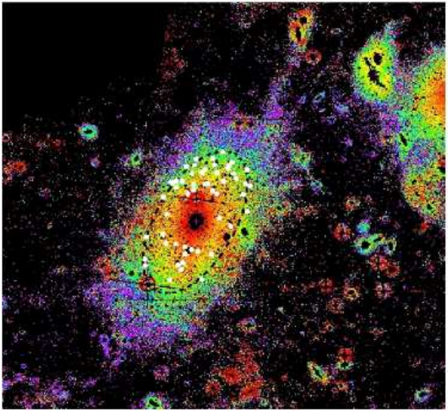

M87 (B-V) colour map (Mihos+15) with Chevron PN overplotted

- Correspondence to blue colours: (B-V)=0.76±0.05
- $\alpha = 1.8 \pm 0.7 \times 10^{-8}$ $N_{PN} L^{-1}_{\odot,bol}$, $L_V = 2.8 \pm 1 \times 10^9 L_{\odot,V}$, M= $6.4 \pm 2.3 \times 10^9 M_\odot$ (Longobardi+15c)

Summary

- We carried out a photometric and spectroscopic PN survey around the dominant elliptical galaxy M87 out to 150 kpc
- The M87 stellar halo is distinct from the surrounding ICL and cannot be considered as a single entity reflected by a gradual transition in kinematics.
- The halo is more centrally concentrated and more steep than the ICL component.
- The observed properties of the halo and IC PN population, such as the α-parameter and the shape of the PNLF show that they have different underlying stellar populations with the halo being redder and more metal rich.
- The progenitors of the stars in the steeper profile (relaxed component) are the most massive systems accreted at higher redshifts, while the stars in the more shallower more extended ICL (unrelaxed component) come from the accretion of smaller systems, accreted at lower redshift.
- The PN phase-space shows signatures of a chevron-like substructure that can be seen in both surface brightness and colour maps.
- M87 is still growing by accreting satellite galaxies.

Summary and Conclusion

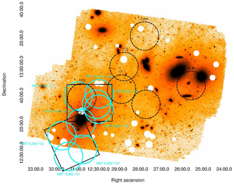

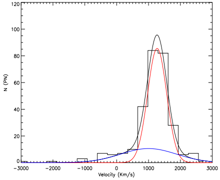

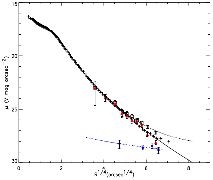

- The M87 stellar halo is distinct from the surrounding ICL and can not be considered as a single entity reflected by a gradual transition in kinematics.
- The observed properties of the halo and IC PNe, such as the α-parameter and the shape of the PNLF show that they have different underlying stellar populations with the halo being more red and more metal rich.
- The progenitors of the stars in the steeper profile (halo, relaxed component) are the most massive systems accreted at higher z, while the stars in the shallower more extended ICL (unrelaxed component) come from the accretion of smaller systems, accreted at lower z.

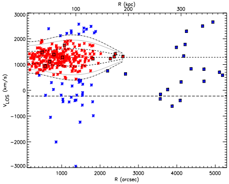

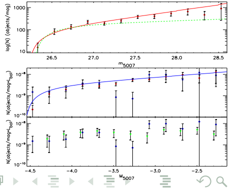

Extraction of Point Like Emission-Line Objects

Point- Like vs Extended Sources

At the distance of 15 Mpc PNe become unresolved points of green light

Criteria for Point-like sources:

- Concentration parameter ($m_n - m_{core}$) in the region defined by simulated point-like objects (bottom left)
- R_h range for point-like objects as defined by simulated sources (bottom right)

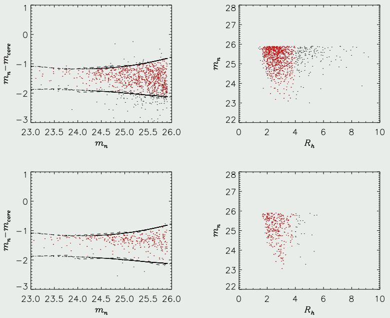

m_{core}: measured magnitude in a fixed aperture of radius $R = 2$ pixels.

R_h: radius within which half of the object's total flux is contained.

Final Catalogue Extraction

Colour selection

Point-like selection

Masking of Compromised regions

Validation of the Catalogue: Visual Inspection

Extraction of 688 PNe candidates

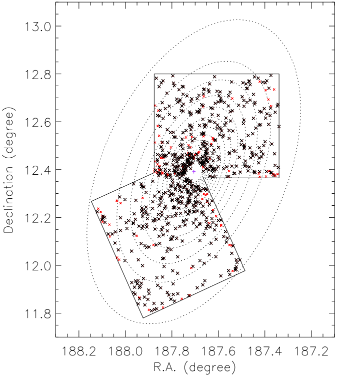

Colour and Spatial Completeness

Galaxy background as well as bright foreground stars affect the detection of emission sources

$\Longrightarrow$ 0.8 average completeness factor

($C_R = 0.8$)

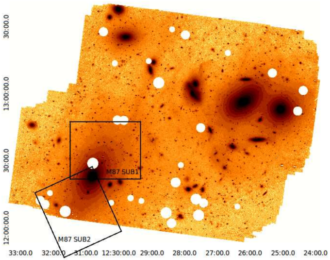

CMD for a simulated PNe population with $23 \leq m_n \leq m_{lim,n}$ (crosses)

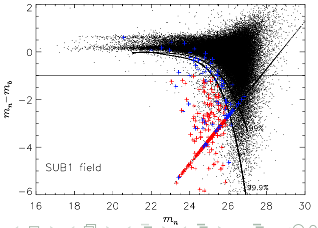

of detected objects : crosses represents simulated candidates that would be selected as PNe (red) or rejected (blue) according to our selection criteria

$\Longrightarrow$ 28,6% of simulated objects with $EW_{obs} < 110$ Å, $m_n \geq m_{lim,n}$, and not point-like.

($C_{phot} = 0.7$)

Contamination by faint continuum objects and background galaxies

- Foreground stars contamination
  Below the 99.9% line the fraction of spurious detection drops to 0.1%.
  $\Longrightarrow$ 10% of misclassified continuum sources in the extracted sample
  - Lyα at $z \sim 3.1$ contamination
    Number density of $z = 3.1$ Lyα galaxies from Gronwall et al 2007. Using their Schechter LF and assuming a constant Lyα distribution
    $\Longrightarrow \sim 25\% \pm 5\%$: Ly$\alpha$ contaminants in our effective volume
  - OII λ3727.26 emitters at $z \sim 0.34$ contamination
    Possible [OII] emitters included in the Gronwall et al. (2007) LF

$\Longrightarrow$ 65% of emission sources are PNe candidates

Comparison with previous PN samples in M87

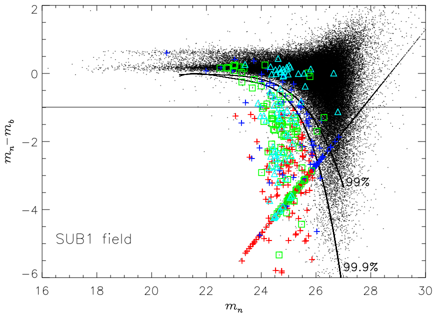

CMD for candidates from C98 (green squares) and F03 (cyan triangles)

By matching our catalogue with the one in literature we find that only $\sim$ 60% of sources from Ciardullo et al. 1998 satisfy our selection criteria for PN candidates. This percentage is even less ($\sim$ 42%) for candidates from Feldmeir et al. 2003.

PNe Spatial Distribution and Surface Density profile

PNe Spatial distribution: PN Number Density

Ellipses: M87's isophotes, $2.8' \leq R \leq 40.7'$
Major-Axis P.A.=-25.6°
(Kormendy et al. 2009)

$$\Sigma_{\mathrm{PNe}}(R) = \frac{N_c(R)}{A(R)}$$

$$\mathrm{N_c(R)} = \frac{\mathrm{N_{obs}(R)}}{\mathrm{C_R} C_{\mathrm{phot}}}$$

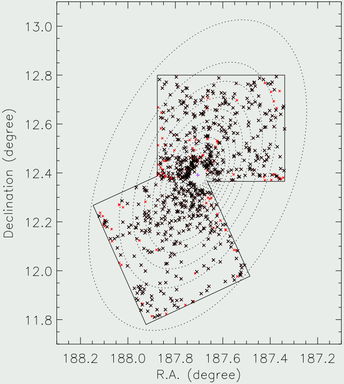

The α-parameter

Hypothesis: Luminosity-specific stellar death rate insnsitive to the population's age, initial mass function, and metallicity
(Renzini & Buzzoni 1986).

$$N_{PN} = B L_{TOT} \tau_{PN}$$

L_{TOT} total bolometric luminosity [$L_\odot$]
B specific evolutionary flux [stars yrs^{-1} $L_\odot^{-1}$]
τ_{PN} PNe visibility lifetime [yrs]

$$\alpha = \frac{N_{PN}}{L_{TOT}} = B\tau_{PN}$$

Luminosity-specic PN number

Observational and theoretical α distribution as function of the (B-V) colour (Buzzoni+06)

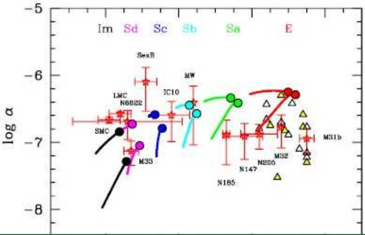

Two components photometric model

$$\tilde{\Sigma}(R) = [\alpha_{2,5,\mathrm{halo}} I(R)_{\mathrm{halo}} + \alpha_{2,5,\mathrm{ICL}} I_{\mathrm{ICL}}]$$

$$I_{\mathrm{K09}} = I_{\mathrm{halo}} + I_{\mathrm{ICL}}$$

$$\tilde{\Sigma}(R) = \alpha_{2,5,\mathrm{halo}} \left[I(R)_{\mathrm{K09}} + \left(\frac{\alpha_{2,5,\mathrm{ICL}}}{\alpha_{2,5,\mathrm{halo}}} - 1 \right) I_{\mathrm{ICL}} \right]$$

Two-component photometric model

$$\mu_{\mathrm{PNe}}(R) = -2.5 \log_{10} \tilde{\Sigma}(R) + \mu_0$$

$$\mu_0 = 2.5 \log_{10} \alpha_{2,5,\mathrm{halo}} + 26.4 + (BC_{\odot} - BC)$$

Modelled SB

$\tilde{\Sigma}(R)$ PNe surface density$[N_{\mathrm{PNe}} pc^{-2}]$
$I(R)$ surface brightness $[L_{\odot} pc^{-2}]$
BC_V=-0.85 V-band bolometric correction (Buzzoni et al 2006)
$BC_{\odot}$=-0.07 Sun bolometric correction

M87 Planetary Nebula Luminosity Function: Radial Variation

triangle: $R \leq 6.5'$

diamonds: $6.5' \leq R \leq 13.5'$

squares: $R \geq 13.5'$

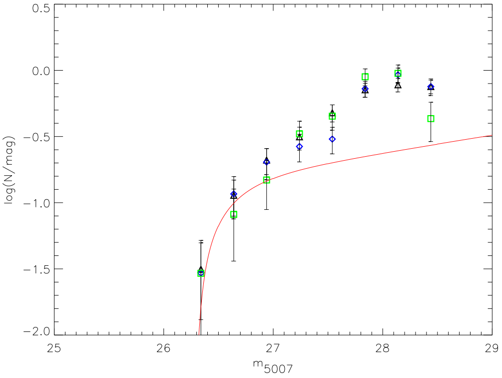

- Steepening observed in all radial bins
- From KS test the three PNLFs are extracted from the same distribution ($P_{KS} > 99\%$)

M87 Planetary Nebula Luminosity Function: Generalised Model for the halo component

$$\frac{\mathrm{N_{halo}}(m)}{\mathrm{N_{tot}}(m)} = \frac{\alpha_{2.5,\mathrm{halo}} L_{\mathrm{halo}}}{\alpha_{2.5,\mathrm{halo}} L_{\mathrm{halo}} + \alpha_{2.5,\mathrm{ICL}} L_{\mathrm{ICL}}} = \frac{1}{1 + 3\frac{L_{\mathrm{ICL}}}{L_{\mathrm{halo}}}}$$

$$N_{\mathrm{halo}}(m) \propto e^{c_2 m} \left\{1 - e^{3(m^* - m)}\right\}$$

$$m^* = 26.3$$
$$c_2 = 1.17$$
$$\chi^2_{\mathrm{red}} = 1.01$$

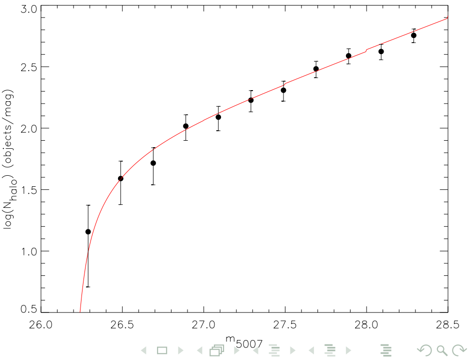

Luminosity normalised M31 and M87 PNLF (photometric results)

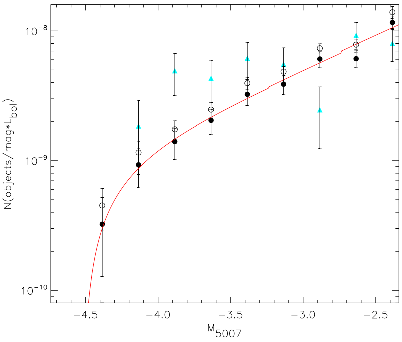

M31 PNLF (cyan triangles, Ciardullo et al. 1989)
M87 PNLF (filled circles)

The slope of the M87 PNLF is steeper towards faint magnitudes, consitent with a larger fraction of PNe with low mass cores

$M_{core} \leq 0.55 M_{\odot}$

Name	Distance (Mpc)	$L_{\odot,bol}$ / $L_{\odot,bol}$	$(B-V)_0$	[Fe/H][a]	$\alpha_{2.5}$	Age[a] Gyr	Ref
M31 (bulge)	0.76[1]	6.5×10^{9}	0.95	$\sim$ 0.	16.3×10^{-9}	> 10	(1)
M87 (halo)	15.0	6.2×10^{10}	0.93	$\sim$ 0.	8.2×10^{-9}	> 10	(2)

(1) Buzzoni et al. 2006
(2) Longobardi et al. 2013
[a] Ratio [Fe/H] and Age from Saglia et al. 2010(M31) and Liu et al. 2005 (M87). M87 [Fe/H] and Age analysis covers the first 400".